Time-Domain Radiation From Large Two-Dimensional Apertures via Narrow-Waisted Gaussian Beams

Vincenzo Galdi, *Member, IEEE*, Leopold B. Felsen, *Life Fellow, IEEE*, and David A. Castañon, *Senior Member, IEEE*

***Abstract*—This paper deals with the short-pulse radiation of three-dimensional (3-D) vector electromagnetic fields from arbitrarily polarized large two-dimensional (2-D) truncated aperture distributions, which are parameterized in terms of narrow-waisted ray-like pulsed Gaussian basis beams centered on a discretized Gabor lattice in a four-dimensional (4-D) configuration-spectrum phase space. The study extends our previous Gabor-based investigation of time-domain (TD) short-pulse radiation of 2-D fields from 1-D large truncated apertures with nonphased, linearly phased (delayed) and nonlinearly phased focusing aperture field profiles [1]. We begin with, and summarize, a Gabor-based frequency domain (FD) formulation of the 2-D aperture problem which has been presented and tested elsewhere [2], [3], but we include additional numerical examples for validation and quality assessment. As in [1], we access the time domain by Fourier inversion from the FD, starting from the initial 3-D space-time Kirchhoff formulation (whose numerical integration furnishes reference solutions), and then passing on to Gabor-parameterized field representations in terms of pulsed beam (PB) wavepackets which are launched by linearly and nonlinearly phase-delayed focusing aperture distributions. Example calculations and comparisons with numerically generated reference data serve to calibrate the Gabor-PB algorithms and assess their domains of validity.**

***Index Terms*—Gabor lattice representations, Gaussian beams, pulsed beam wavepackets.**

I. Introduction

In an ongoing series of recent investigations, we have revisited a previously formulated discretized Gabor-based narrow-waisted Gaussian beam (GB) algorithm for two-dimensional (2-D) time-harmonic high-frequency radiation from truncated one-dimensional (1-D) planar aperture distributions [4], which was then applied to the interaction of these GB-parameterized radiated fields with complex propagation environments [5], [6]. The algorithm had been found to be robust, accurate, physically appealing, and numerically efficient when compared with conventional Kirchhoff Physical Optics integration procedures. Our recent interest has been motivated in part by the need of robust forward solvers in forward and inverse scattering (identification and imaging) scenarios concerned with objects embedded within an irregularly bounded penetrable semi-infinite medium. In a stepwise approach toward constructing the necessary algorithms, we have proceeded along two parallel routes: 1. extension of the frequency domain (FD) algorithms for the 1-D aperture/2-D field configuration to the new rough interface propagation environment, and to the new general case of 2-D aperture/three-dimensional (3-D) vector fields; 2. extension of the FD results to the short-pulse-excited time domain (TD). The FD interaction of the 1-D aperture radiated field with a moderately rough interface has been addressed in [7] and [8] for the forward problem and in [9] and [10] for the inverse problem, whereas the 2-D aperture/3-D field radiation problem has been addressed in [2] and [3]. The TD extension of the 1-D aperture problem has been carried out in [1], and the extension to 2-D apertures is the subject of the present paper. The contents of this paper having been summarized in the abstract, we pass on directly to the problem formulation and its solution via the Gabor-based narrow-waisted beam algorithm.

Manuscript received January 11, 2001; revised August 22, 2001. This work was supported by ODDR&E under MURI Grants ARO DAAG55-97-1-0013 and AFOSR F49620-96-1-0028, and by the Engineering Research Centers Program of the National Science Foundation under Award number EEC-9986821. The work of V. Galdi was also supported by a European Union Postdoctoral fellowship through the University of Sannio, Benevento, Italy. The work of L. B. Felsen was also supported in part by Grant 9900448 of the U.S.-Israel Binational Science Foundation, Jerusalem, Israel, and from Polytechnic University, Brooklyn, NY 11201 USA.

V. Galdi was with the Department of Electrical and Computer Engineering, Boston University, Boston, MA 02215 USA. He is now with the Department of Engineering, University of Sannio, Benevento, Italy (e-mail: vgaldi@unisannio.it).

L. B. Felsen is with the Department of Aerospace and Mechanical Engineering and the Department of Electrical and Computer Engineering, Boston University, Boston, MA 02215 USA. He is also Professor Emeritus, Polytechnic University, Brooklyn, NY 11201 USA (e-mail: lfelsen@bu.edu).

D. A. Castañon is with the Department of Electrical and Computer Engineering, Boston University, Boston, MA 02215 USA (e-mail: dac@bu.edu).

Digital Object Identifier 10.1109/TAP.2003.808520

II. Formulation of the Problem

We consider the radiation of three-dimensional (3-D) vector electromagnetic (EM) fields excited by pulsed arbitrarily polarized extended two-dimensional (2-D) vector field distributions in a truncated planar aperture of characteristic dimension d_A on the $z = 0$ plane of Fig. 1. We shall only deal with the vector electric field $\mathbf{e}(\mathbf{r}, t)$, $\mathbf{r} = x\mathbf{u}_x + y\mathbf{u}_y + z\mathbf{u}_z$; the vector magnetic fields can be derived from Maxwell's equations. Here and henceforth, bold face symbols denote vector quantities, and $\mathbf{u}_\alpha$ denotes a unit vector in the α-direction. The 2-D space–time aperture field distribution will be specified as

$$\mathbf{e}_0(x, y, z = 0, t) = \mathbf{f}(x, y, t),\ (x, y) \in \Gamma_A, \quad \mathbf{u}_z \cdot \mathbf{f} = 0. \quad (1)$$

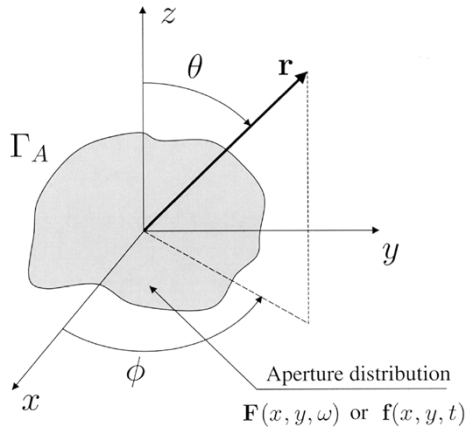

Fig. 1. 2-D aperture field distribution and coordinate systems.

The corresponding field radiated into the half-space $z > 0$ can be obtained by space-time superposition, using the 3-D TD Green's function

$$g_{3-D}(\mathbf{r},t;\mathbf{r}_0',t') = \frac{\delta\left(t-t'-\frac{R}{c}\right)}{4\pi R},\ R=|\mathbf{r}-\mathbf{r}_0'| \quad (2)$$

where $\mathbf{r}_0' = x'\mathbf{u}_x + y'\mathbf{u}_y$, $\delta(\cdot)$ represents the Dirac delta function, and c is the ambient propagation speed. The subscript "$_0$" identifies quantities in the $z = 0$ plane. The resulting field radiated into the half-space $z > 0$, synthesized by superposition of point source contributions (Kirchhoff integration), is given by [11, p. 175] (see (3) at the bottom of the page). In Section IV-D, we shall be using a reference solution based on Gaussian quadrature numerical integration [12] of (3). In what follows, the time domain is accessed by Fourier inversion from the FD via the Fourier transform pair

$$\begin{aligned}\mathbf{e}(\mathbf{r},t) =& \frac{1}{2\pi}\int_{-\infty}^{\infty}\mathbf{E}(\mathbf{r},\omega)\exp(-i\omega t)d\omega,\ \mathbf{E}(\mathbf{r},\omega)\\ =& \int_{-\infty}^{\infty}\mathbf{e}(\mathbf{r},t)\exp(i\omega t)dt.\end{aligned} \quad (4)$$

Capital letters identify FD field quantities.

III. Relevant FD Results

This section contains a brief summary of relevant FD results from [2], [3] and some new additions. The FD aperture field corresponding to (1) has an implicit $\exp(-i\omega t)$ time dependence and a spatial distribution $\mathbf{F}(x,y,\omega)$ [related to $\mathbf{f}$ via the Fourier transform pair in (4)] over the aperture Γ_A in Fig. 1,

$$\mathbf{E}_0(x,y,z=0,\omega) = \mathbf{F}(x,y,\omega),\quad (x,y)\in\Gamma_A,\quad \mathbf{u}_z\cdot\mathbf{F}=0. \quad (5)$$

The resulting electric field in the half-space $z > 0$, obtained by point-source (Kirchhoff) integration in configuration space, is given by [11, p. 107]

$$\begin{aligned}&\mathbf{E}(\mathbf{r},\omega)\\ &= 2\int_{-\infty}^{\infty}\int_{-\infty}^{\infty}\nabla G_{3-D}(\mathbf{r},\mathbf{r}_0';\omega)\times[\mathbf{u}_z\times\mathbf{F}(x',y',\omega)]\,dx'dy'\end{aligned} \quad (6)$$

where

$$G_{3-D}(\mathbf{r},\mathbf{r}_0';\omega) = \frac{\exp(ikR)}{4\pi R},\quad R=|\mathbf{r}-\mathbf{r}_0'| \quad (7)$$

is the 3-D free-space FD Green's function, with $k = \omega/c = 2\pi/\lambda$ as the ambient wavenumber and λ as the wavelength. It can easily be verified (see [11, p. 175]) that $\mathbf{e}(\mathbf{r},t)$ in (3) and $\mathbf{E}(\mathbf{r},\omega)$ in (6) are related through the Fourier transform pair (4). In the remainder of this section, the ω dependence in $\mathbf{E}$ and $\mathbf{F}$ will be omitted for simplicity of notation, and the discussion relies heavily on references [1]–[3], with precise citations attached to each of the results extracted from these papers. Notationally, we use (2.5) to identify [2, eq. (5)], for example. We also call attention to the following differences between [2], [3] and the present paper: 1. [2] and [3] deal with the calculation of the vector potential $\mathbf{P}$ whereas here we calculate the vector field $\mathbf{E}$. 2. The aperture potential field in [2] and [3] is denoted by $\mathbf{f}$ which should not be confused with the TD $\mathbf{f}$ in (1) here. These differences do not affect the *basic format* of the Gabor expansions to which the citations refer.

A. Discretized Gabor-Based Field Representations in the Configuration-Spectrum Phase Space

1) Aperture Field: The vector aperture field $\mathbf{F}(x,y)$ can be expressed in the 2-D Gabor Gaussian beam (GB) basis as follows [see (2.4)]

$$\begin{aligned}\mathbf{F}(x,y) =& \\ &\sum_{m,n,p,q=-\infty}^{\infty}\mathbf{A}_{mnpq}w(x-mL_x,y-pL_y)\\ &\exp\left[i\left(n\beta_x x+q\beta_y y\right)\right]\end{aligned} \quad (8)$$

with $w(x,y)$ representing the normalized 2-D Gaussian window in (2.10a), [see (9) at the bottom of the next page]. The representation in (8) is tied to a 4-D lattice in the $(x,y;k_x,k_y)$ phase-space (Fig. 2), k_x, k_y being the x and y-domain wavenumbers, respectively, which can be expressed in terms of the spherical polar coordinate angles θ, ϕ (see Fig. 1) as

$$\begin{aligned}k_x =& k\sin\theta\cos\phi,\ k_y = k\sin\theta\sin\phi\\ k_z =& \sqrt{k^2-k_x^2-k_y^2} = k\cos\theta.\end{aligned} \quad (10)$$

$$\mathbf{e}(\mathbf{r},t) = -\frac{1}{2\pi}\int_{-\infty}^{\infty}\int_{-\infty}^{\infty}(\mathbf{r}-\mathbf{r}_0')\times\left\{\mathbf{u}_z\times\left[\frac{\mathbf{f}\left(x',y',t-\frac{R}{c}\right)}{R^3}+\frac{1}{cR^2}\frac{\partial}{\partial t}\mathbf{f}\left(x',y',\frac{t-R}{c}\right)\right]\right\}dx'dy'. \quad (3)$$

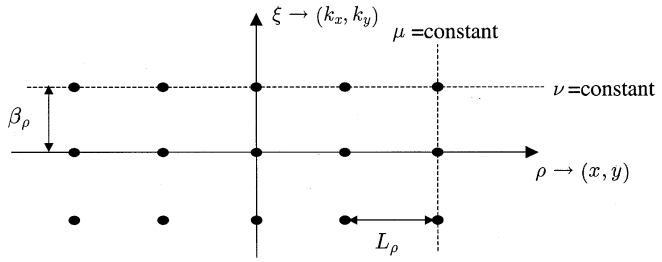

Fig. 2. 2-D projection of the 4-D $(x, y; k_x, k_y)$ discretized Gabor lattice onto 2-D (ρ, ξ) subspaces, where ρ stands for either x or y and ξ stands for either k_x or k_y, with μ and ν denoting the corresponding spatial and spectral integer indexes (m, p) or (n, q), respectively. ν = const.: spatially displaced beams centered at $\rho_\mu = \mu L_\rho$, with fixed phase gradient (beam tilt) $\nu\beta_\rho$; μ = const.: spectrally displaced beam tilts $(\nu\beta_\rho)$ at fixed beam location ρ_μ.

In this Gabor basis, each lattice point locates a GB, whose initial profile matches the corresponding basis function. Indexes (m, p) tag x, y spatial shifts, respectively, whereas (n, q) tag k_x, k_y spectral shifts (i.e., beam tilts θ_{nq}, ϕ_{nq}), respectively. Spatial and spectral periods are related by the self-consistency relation (configuration-spectrum tradeoff) (2.4a)

$$L_x\beta_x = L_y\beta_y = 2\pi. \tag{11}$$

From (10), as the spectral shifts increase, the corresponding (n, q) beam polar angles $\theta_{nq} = \sin^{-1}[(k_x^2 + k_y^2)^{1/2}/k]_{nq}$, i.e.,

$$\begin{aligned}\theta_{nq} &= \sin^{-1}\left[\frac{\sqrt{(n\beta_x)^2 + (q\beta_y)^2}}{k}\right] \\ &= \sin^{-1}\left[\sqrt{\left(\frac{n\lambda}{L_x}\right)^2 + \left(\frac{q\lambda}{L_y}\right)^2}\right]\end{aligned} \tag{12}$$

become *complex* for $[(n\lambda/L_x)^2 + (q\lambda/L_y)^2] > 1$, and therefore the corresponding beams away from the aperture (see Section III-A.II) become *evanescent*. In the second equality of (12), use has been made of (11) and $k = 2\pi/\lambda$.

The expansion coefficients in (8) can be computed by introducing an auxiliary *biorthogonal* function $\gamma(x, y)$ [cf. (2.8)], [see (13) at the bottom of the page] where * denotes the complex conjugate. For the Gaussian window in (9), a closed-form expression for $\gamma(x, y)$ is derived in [2, App. C.] Alternatively, the Gabor coefficients can be computed effectively by schemes employed in image processing [13]. However, we shall avoid this calculation later on by specializing to narrow-waisted Gaussian basis functions (see Section III-B).

2) Radiated Field: The Gabor lattice representation for the field radiated into the half-space $z > 0$ follows by combining (6) and (8)

$$\mathbf{E}(\mathbf{r}) = \sum_{m,n,p,q=-\infty}^{\infty} (\mathbf{A}_{mnpq} \times \mathbf{u}_z) \times \mathbf{B}_{mnpq}(\mathbf{r}) \tag{14}$$

with the (vector) beam propagator $\mathbf{B}_{mnpq}$ expressed by Gabor-weighted point-source superposition as [see (15) at the bottom of the page].

B. Narrow-Waisted Beams

When the observer is located in the *paraxial far-zone* of a beam, the integral in (15) can be evaluated by saddle-point asymptotics. It is shown in [3, Sec. III], that the result can be expressed in an explicit closed form in terms of *complex source point* (CSP) propagators, provided the beams are nontilted $(n = q = 0)$, narrow-waisted $(L_{x,y} \lesssim \lambda \ll d_A)$, and distributed over a symmetric lattice $(L_x = L_y = L)$. Narrow-waisted (ray-like) GBs have been shown in a series of previous studies of 2-D fields excited by 1-D apertures [5]–[8] to yield highly efficient and accurate algorithms for synthesis of interactions with complex propagation and scattering environments. The narrow-waisted nontilted GB can be related to the 3-D-CSP Green's function $\tilde{G}_{3-D}$ as follows: [cf. (3.14)]

$$\tilde{\mathbf{B}}_{m0p0}(\mathbf{r}) \sim 2\sqrt{2}L\exp(-kb)\nabla\tilde{G}_{3-D}(\mathbf{r}, \tilde{\mathbf{r}}'_{mp}) \tag{16}$$

$$\sim ikL\frac{\exp[ik(\tilde{R}_{mp} + ib)]}{\sqrt{2}\pi\tilde{R}_{mp}^2}\left(\mathbf{r} - \tilde{\mathbf{r}}'_{mp}\right) \tag{17}$$

where

$$\begin{aligned}\tilde{R}_{mp} = \left|\mathbf{r} - \tilde{\mathbf{r}}'_{mp}\right| &= \sqrt{(x - x'_m)^2 + (y - y'_p)^2 + (z - \tilde{z}')^2} \\ \mathrm{Re}(\tilde{R}_{mp}) &\geq 0\end{aligned} \tag{18}$$

$$w(x, y) = \left(\frac{2}{L_xL_y}\right)^{1/2}\exp\left\{-\pi\left[\left(\frac{x}{L_x}\right)^2 + \left(\frac{y}{L_y}\right)^2\right]\right\},\ \int_{-\infty}^{\infty}\int_{-\infty}^{\infty} w^2(x, y)dx\,dy = 1. \tag{9}$$

$$\mathbf{A}_{mnpq} = \int_{-\infty}^{\infty}\int_{-\infty}^{\infty}\mathbf{F}(x, y)\gamma^*(x - mL_x, y - pL_y)\exp\left[-i\left(n\beta_x x + q\beta_y y\right)\right]dxdy \tag{13}$$

$$\mathbf{B}_{mnpq}(\mathbf{r}) = 2\int_{-\infty}^{\infty}\int_{-\infty}^{\infty}\nabla G_{3-D}(\mathbf{r}, \mathbf{r}'_0)w(x' - mL_x, y' - pL_y)\exp\left[i\left(n\beta_x x' + q\beta_y y'\right)\right]dx'dy'. \tag{15}$$

is the complex distance between the real observation point $\mathbf{r}$ and the complex source point

$$\tilde{\mathbf{r}}'_{mp} = x'_m \mathbf{u}_x + y'_p \mathbf{u}_y + \tilde{z}' \mathbf{u}_z = mL\mathbf{u}_x + pL\mathbf{u}_y + ib\mathbf{u}_z. \quad (19)$$

Here and henceforth, the tilde $\sim$ identifies dependence on analytically continued spatial source coordinates as well as the field produced thereby. The complex displacement parameter is given by (3.11c)

$$\tilde{z}' = ib, \quad b = \frac{L^2}{\lambda}. \quad (20)$$

One notes that b is the beam Fresnel length corresponding to an "effective" beam waist L. Equation (16) and (17) are valid in the paraxial far-zone of each beam, $|\tilde{R}_{mn}| \gg b$, and are restricted to symmetric and nontilted beams only. However, recalling (12), one observes that these nontilted sufficiently *narrow* beams with $n = q = 0$, $L \lesssim \lambda \ll d_A$, yield the dominant contribution to the radiated field because all other beams are evanescent.

An important attractive feature of narrow-waisted GBs is that their Gabor coefficients can be estimated effectively by *aperture sampling* [see (3.19)], avoiding the time-consuming operations required in (13) and (2.11a,b) or [13]

$$\mathbf{A}_{mnpq} \approx \begin{cases} \left(\frac{L}{\sqrt{2}}\right) \mathbf{F}(mL, pL), & n, q = 0 \\ 0, & n, q \neq 0 \end{cases} \quad (21)$$

so that

$$\tilde{\mathbf{E}}(\mathbf{r}) \sim \sum_{m,p} (\mathbf{A}_{m0p0} \times \mathbf{u}_z) \times \tilde{\mathbf{B}}_{m0p0}(\mathbf{r}). \quad (22)$$

Due to the finite extent of the aperture, the (m, p) summations in (22) include only a finite number of beams, given roughly by $(d_A/L)^2$. The approximation in (21) and (22) neglects the tilted (n, $q \neq 0$) beams in the Gabor expansion which, however, are *evanescent* for $[(n\lambda/L_x)^2 + (q\lambda/L_y)^2] > 1$, as noted earlier. Subject to the constraints $n = q = 0$, $L \lesssim \lambda \ll d_A$, the CSP paraxial *far-zone* approximation (17) can be invoked at *moderate* distance, within and beyond the radiating *near-zone* of the *aperture*. The resulting beam synthesis in (22), with (21) and (17), yields an efficient algorithm which has been tested and validated in Section III-D.

C. Linearly Phased Aperture

For linearly phased distributions, the aperture field becomes

$$\mathbf{F}(x, y) = \mathbf{g}(x, y) \exp\left[ik \sin\theta_A \left(x \cos\phi_A + x \sin\phi_A\right)\right] \quad (23)$$

where $\mathbf{g}(x, y)$ is a real function and θ_A, ϕ_A specify the direction of the main radiation lobe. Now, a more effective implementation of the narrow-waisted beam discretization can be achieved by exploiting *propagation-matched tilted* beams, which has not been investigated in [3]. As for the 2-D field/1-D aperture problem in [1], this is achieved by Gabor-expanding the real function $\mathbf{g}(x, y)$ only, and including the linear phasing in the beam integral (15) for the $\mathbf{B}_{m0p0}$ beam propagator. Accordingly, generalizing the 1-D aperture expressions in (1.18)–(1.20) to the 2-D aperture case, the narrow-waisted beam expansion (22) can be recast as (for simplicity, the subscript "$_{m0p0}$" is, henceforth, replaced by "$_{mp}$")

$$\tilde{\mathbf{E}}(\mathbf{r}) \sim \sum_{m,p} (\mathbf{C}_{mp} \times \mathbf{u}_z) \times \tilde{\mathcal{B}}_{mp}(\mathbf{r}) \quad (24)$$

where

$$\mathbf{C}_{mp} \approx \left(\frac{L}{\sqrt{2}}\right) \mathbf{g}(mL, pL) \quad (25)$$

$$\tilde{\mathcal{B}}_{mp}(\mathbf{r}) = ikL \frac{\exp[ik(\tilde{R}_{mp} + ib + \mathcal{L}_{mp})]}{\sqrt{2}\pi \tilde{R}^2_{mp}} (\mathbf{r} - \tilde{\mathbf{r}}'_{mp}) \quad (26)$$

$$\mathcal{L}_{mp} = L \sin\theta_A \left(m \cos\phi_A + p \sin\phi_A\right) \quad (27)$$

$$\tilde{R}_{mp} = \left|\mathbf{r} - \tilde{\mathbf{r}}'_{mp}\right| \quad (28)$$

$$\begin{aligned} \tilde{\mathbf{r}}'_{mp} &= \tilde{x}'_m \mathbf{u}_x + \tilde{y}'_p \mathbf{u}_y + \tilde{z}' \mathbf{u}_z = \\ &= (mL + ib \sin\theta_A \cos\phi_A)\mathbf{u}_x \\ &\quad + (pL + ib \sin\theta_A \sin\phi_A)\mathbf{u}_y + ib \cos\theta_A \mathbf{u}_z \end{aligned} \quad (29)$$

$$b = \frac{(L \cos\theta_A)^2}{\lambda}. \quad (30)$$

Instead of $\mathbf{A}_{mp}$, $\mathbf{C}_{mp}$ in (24) and (25) identifies Gabor coefficients associated with the tilt-matched linearly phased aperture formulation. The beam propagator (26) differs from $\tilde{\mathbf{B}}_{m0p0}$ in (17) by the phase shift ($ik\mathcal{L}_{mp}$) and by the different definitions of the CSP $\tilde{\mathbf{r}}'_{mp}$ and b in (29) and (30), respectively, [see (1.21) and (1.22)], which produce the propagation-matched tilt (θ_A, ϕ_A) in the beam direction. Equation (26) can be obtained by the same procedure that leads to (17), or even by inspection, recalling the 1-D aperture results [1]. As shown in Section III-D below, for linearly phased apertures, the tilted beam expansion (24) allows significantly coarser lattice sampling than (22), for the same degree of accuracy. For *moderately* nonlinear phasing it may still be convenient to split the phase function into a linear term (included in the beam propagator as above) and a nonlinear remainder (included in the Gabor-expanded function $\mathbf{g}$), but no particular benefit is expected for *strongly* nonlinear phasing (e.g., strongly focused apertures).

D. Numerical Results

In order to compare the nontilted and tilted formulations in (22) and (24), respectively, we consider the linearly phased distribution in (23), with an x polarized tapered square cosine amplitude distribution

$$\mathbf{g}(x, y) = \begin{cases} \cos\left(\frac{\pi x}{d_A}\right) \cos\left(\frac{\pi y}{d_A}\right) \mathbf{u}_x, & |x|, |y| \leq \frac{d_A}{2} \\ 0, & |x|, |y| > \frac{d_A}{2} \end{cases}. \quad (31)$$

It follows from (6), that the resulting vector electric field radiated into the $z > 0$ half-space has x, z components only. All other parameters used in our simulations are listed in the figure captions. In our simulations, we assume $\theta_A = 30°$, $\phi_A = 45°$, and a fixed (symmetric) beam lattice period ($L_x = L_y = L = 0.8\lambda$).

In Fig. 3(a) and (b), the x components of the radiated fields synthesized under the same conditions with the same number ($(d_A/L)^2 \sim 150$) of narrow-waisted nontilted (22) and tilted (24) beams are compared with the reference solution (Gaussian

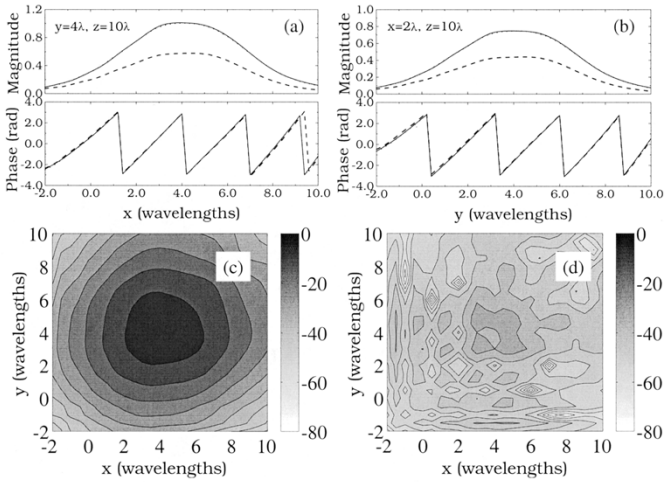

Fig. 3. x polarized, linearly-phased, square cosine aperture distribution in (23) with (31) ($d_A = 10\lambda$, $\theta_A = 30°$, $\phi_A = 45°$): **x component** of near-zone ($z = 10\lambda$) radiated field synthesis using narrow-waisted nontilted and tilted beams with a fixed beam lattice period ($L = 0.8\lambda$) is compared with the reference solution (numerical integration of (6)). The number of beams used is $(d_A/L)^2 \sim 150$. (a) Cut at $y = 4\lambda$. (b) Cut at $x = 2\lambda$; —— Reference solution; – – – Nontilted beam synthesis; ····· Tilted beam synthesis. The reference solution and tilted beam synthesis coincide on the scale of plots. (c), (d) Grayscale plots of the relative error (32) (in dB) for nontilted and tilted beam synthesis, respectively.

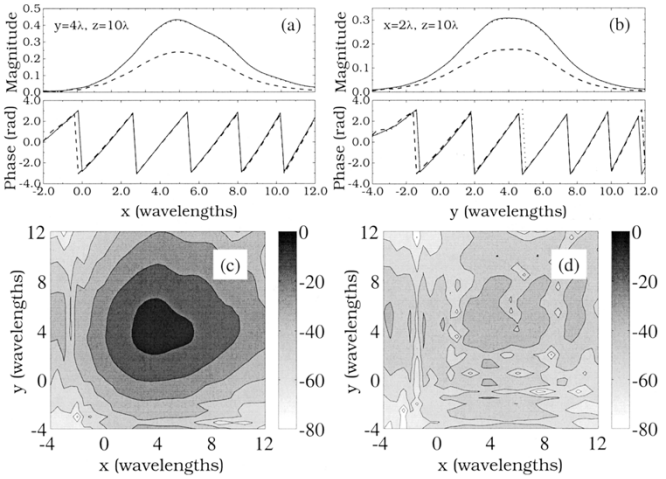

Fig. 4. As in Fig. 3, but **z component**.

quadrature numerical integration of (6)), showing representative x and y cuts, respectively, at a fixed value of z well within the aperture near-zone. The tilted beam synthesis is barely distinguishable from the reference solution, whereas the nontilted synthesis is noticeably more *inaccurate*. The accuracy is more clearly quantified in Fig. 3(c) and (d), where the relative error magnitudes

$$\Delta E_{x,z} \equiv \frac{\left| E_{x,z}^{(ref)} - E_{x,z}^{(beam)} \right|}{\max \left| E_{x,z}^{(ref)} \right|} \tag{32}$$

are displayed as grayscale plots. It is observed that the tilted beam synthesis attains a maximum error < -30 dB, whereas the nontilted beam synthesis error is evidently greater. In order to obtain comparable accuracy with nontilted beams, a considerably smaller beam lattice period ($L \sim 0.1\lambda$) should be used, resulting in an overall computation time increase of almost *two orders of magnitude*. The corresponding results for the z component are shown in Fig. 4, and the same considerations apply. The nonphased case ($\theta_A = 0$) yields the same results as in [3].

As a further more challenging test, we consider a *quadratically phased*, cosine-tapered aperture field distribution

$$\mathbf{F}(x,y) = \mathbf{g}(x,y) \exp\left[-ik \frac{(x^2+y^2)}{2L_f} \right] \tag{33}$$

with $\mathbf{g}(x,y)$ defined in (31), which produces focusing ($L_f > 0$) or defocusing ($L_f < 0$), with L_f representing the conventional focal length. Fig. 5(a) shows the magnitude profile plot of the x component of radiated electric field at the focal plane

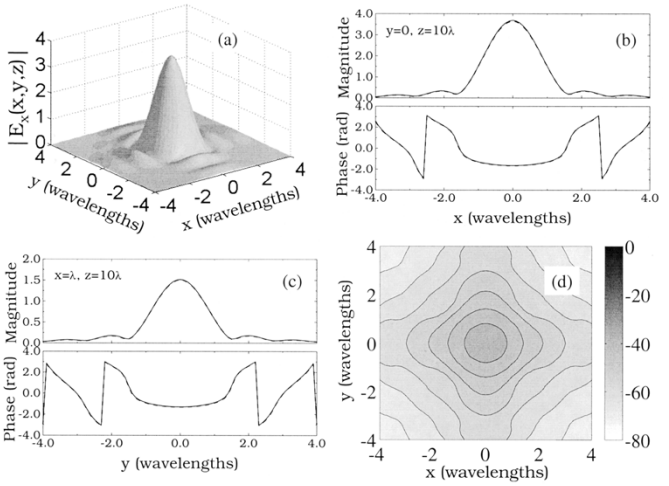

Fig. 5. x polarized, focused, square cosine aperture distribution in (33) ($d_A = 10\lambda$, $L_f = 10\lambda$): **x component** of radiated field at the focal plane $z = L_f$. (a) Magnitude profile plot of the reference solution (numerical integration of (6)). (b),(c) Cuts at $y = 0$ and $x = \lambda$, respectively, comparing the reference solution with the narrow-waisted beam synthesis ((22) with $L = 0.2\lambda$). (d): Gray-scale plot of the relative error (32) (in dB) for the beam synthesis ($L = 0.2\lambda$). The number of beams used is $(d_A/L)^2 \sim 2500$. —— Reference solution; – – – Beam synthesis.

$z = L_f > 0$ (chosen well within the aperture near-zone), computed via numerical Kirchhoff integration of (6). The wavefield is peaked around the point $(x,y) = (0,0)$, clearly highlighting the focusing effects. Fig. 5(b) and (c) shows representative x and y cuts, respectively, where the reference solutions are compared with the narrow-waisted beam synthesis (22). Note that, as compared with the linearly phased example, a smaller beam lattice period with a correspondingly larger number of beams ($(d_A/L)^2 = 2500$) is required for the strongly nonlinear phasing in order to attain comparable accuracy. As shown in Fig. 5(d), a value $L = 0.2\lambda$ suffices to keep the maximum error below -30 dB. The corresponding results for the z component are shown in Fig. 6, and the same conclusions hold. It should be emphasized that the near-zone focal plane field poses a relatively strong challenge; for moderate observation distances away from the focal plane, a coarser discretization is adequate.

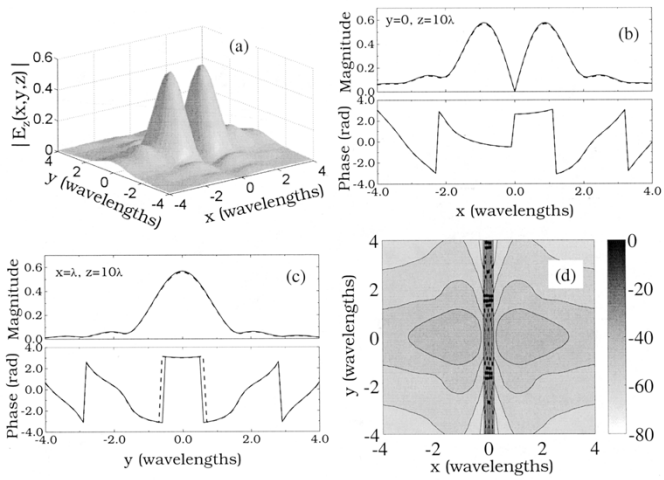

Fig. 6. As in Fig. 5, but **z component**.

IV. TD Formulation

A. TD Narrow-Waisted Beam Discretization: Linear-Delay Aperture Fields

Rigorous extension, into the TD, of the GB discretization for the time-harmonic aperture distribution in Section III would require a six-index Gabor series tied to a discretized lattice in the six-dimension (6-D) (space-time, wavenumber-frequency) phase space. However, for the narrow-waisted beams in Section III-B, which we shall use throughout, implementation of the Gabor algorithm simplifies substantially. In particular, we extend the TD formulation for 2-D field radiation by 1-D pulsed aperture distributions in [1] to pulsed radiation from 2-D aperture distributions. As in [1, Sec. III-A], generalizing (1.28), we first consider space-time separable aperture fields with linear time delay and θ_A, ϕ_A real,

$$\mathbf{f}(x,y,t) = \mathbf{g}(x,y)p[t - c^{-1}\sin\theta_A(x\cos\phi_A + y\sin\phi_A)] \tag{34}$$

and its FD counterpart via (4)

$$\mathbf{F}(x,y,\omega) = P(\omega)\mathbf{g}(x,y)\exp[ik\sin\theta_A(x\cos\phi_A + y\sin\phi_A)]. \tag{35}$$

Here, $p(t)$ is a pulse of short length with respect to the characteristic aperture width d_A, i.e., $T \ll d_A/c$, and $P(\omega)$ is its Fourier transform

$$P(\omega) = \int_{-\infty}^{\infty} p(t)\exp(i\omega t)dt. \tag{36}$$

The results in this section are related to those in Section III through the Fourier transform in (4) filtered by the pulse spectrum $P(\omega)$. When the aperture field is expressed in the Gabor representation based on the CSP beam propagator in (26), the presence of its evanescent spectra motivates use of the one-sided analytic transform [11, p. 222] as in [1]

$$\overset{+}{f}(t) = \frac{1}{\pi}\int_0^{\infty} F(\omega)\exp(-i\omega t)d\omega,\ \mathrm{Im}(t) \le 0 \tag{37}$$

where $F(\omega)$ is the conventional Fourier spectrum of the real signal $f(t)$ [see (4)], and the real signal for real t is recovered via

$$f(t) = \mathrm{Re}\left[\overset{+}{f}(t)\right]. \tag{38}$$

Then by FD inversion of (24)

$$\overset{+}{e}(\mathbf{r},t) \sim \sum_{m,p}(\mathbf{c}_{mp}\times\mathbf{u}_z)\times\overset{+}{\mathbf{b}}_{mp}(\mathbf{r},t) \tag{39}$$

with $\mathbf{c}_{mp} = \mathbf{C}_{mp}$ in (25), and the analytic pulsed beam (PB) propagator $\overset{+}{\mathbf{b}}_{mp}$ expressed via (37) in terms of the paraxial, far-zone FD propagator $\tilde{\mathcal{B}}_{mp}$ in (26) as

$$\overset{+}{\mathbf{b}}_{mp}(\mathbf{r},t) = \frac{1}{\pi}\int_0^{\infty}\tilde{\mathcal{B}}_{mp}(\mathbf{r},\omega)P(\omega)\exp(-i\omega t)d\omega,\ \mathrm{Im}(t)\le 0. \tag{40}$$

To simplify the evaluation of the integral in (40), it has been customary to choose the complex displacement ib in (26) to be frequency independent so as to yield "isodiffracting" basis beam wavepackets which remain collimated over a range of frequencies [14]. Via (30), the isodiffracting excitation requires a frequency-dependent beam lattice. However, as noted before (see also [1]), this leads to frequency-dependent Gabor coefficients which cannot be computed by aperture profile sampling when the narrow-waisted constraint is imposed. We therefore choose L to be frequency independent, to obtain the approximate Gabor coefficients

$$\mathbf{c}_{mp} = \mathbf{C}_{mp} \approx \left(\frac{L}{\sqrt{2}}\right)\mathbf{g}(mL,pL) \tag{41}$$

but at the expense of a frequency-dependent b, which is dealt with below. From here on, we continue by generalizing the 1-D aperture algorithm in [1], and consider a class of differentiated Gaussian pulses [cf. (1.37) and (1.38)]

$$p(t) = P_0 p_g^{(j)}\left(t - \frac{T}{2}, T\right), \tag{42}$$

$$P(\omega) = P_0(-i\omega)^j\exp\left(i\omega\frac{T}{2}\right)P_g(\omega,T) \tag{43}$$

where P_0 is a normalization constant, the superscript $^{(j)}$ indicates jth-order differentiation with respect to t, and $p_g(t)$, $P_g(\omega)$ denote the standard Gaussian pulse and its spectrum, respectively,

$$p_g(t,T) = \exp\left[-\left(\frac{t}{\sigma T}\right)^2\right],$$
$$P_g(\omega,T) = \sqrt{\pi}\sigma T\exp\left(-\frac{\sigma^2T^2\omega^2}{4}\right) \tag{44}$$

the variance σ is chosen so that the pulse width of $p(t)$ is $\sim T$.

To deemphasize the effect of the frequency-dependent parameter b on the complex distance $\tilde{R}_{mp}$ in (28), we assume L/λ

(and therefore, b) sufficiently small, so that the resulting amplitude factor in the FD beam propagator (26) can be approximated by [see (29) or (1.39)]

$$\frac{\mathbf{r}-\tilde{\mathbf{r}}'_{mp}}{\tilde{R}_{mp}} \approx \frac{\mathbf{r}-\mathbf{r}'_{mp}}{R_{mp}}, \mathbf{r}'_{mp} = mL\mathbf{u}_x + pL\mathbf{u}_y,$$
$$R_{mp} = \left|\mathbf{r}-\mathbf{r}'_{mp}\right|, \ \frac{b}{L} = \frac{L(\cos\theta_A)^2}{\lambda} \ll 1 \quad (45)$$

where the source point $\mathbf{r}'_{mp}$ and the distance R_{mp} are now *real* and *frequency independent*. In the phase, under the same assumptions, we retain the first order paraxial correction [extending (1.40)]

$$\tilde{R}_{mp} \approx z_{bmp} - ib + \frac{\rho_{bmp}^2}{2(z_{bmp}-ib)}$$
$$\approx z_{bmp} - ib + \frac{\rho_{bmp}^2(z_{bmp}+ib)}{2z_{bmp}^2} \quad (46)$$

subject to [see (1.42) and (1.43)]

$$|z_{bmp}-ib| \gg \rho_{bmp}, \ b = \frac{(L\cos\theta_A)^2\omega}{2\pi c} \ll z_{bmp}, \ \omega \le \Omega. \quad (47)$$

Here, $\rho_{bmp} = (x_{bmp}^2 + y_{bmp}^2)^{1/2}$, Ω denotes the bandwidth of the pulse spectrum $P(\omega)$, and $(x_{bmp}, y_{bmp}, z_{bmp})$ are the 3-D beam coordinates [cf. (1.41)]

$$\begin{bmatrix} x_{bmp} \\ y_{bmp} \\ z_{bmp} \end{bmatrix} = \begin{bmatrix} \cos\theta_A\cos\phi_A & \cos\theta_A\sin\phi_A & -\sin\theta_A \\ -\sin\phi_A & \cos\phi_A & 0 \\ \sin\theta_A\cos\phi_A & \sin\theta_A\sin\phi_A & \cos\theta_A \end{bmatrix} \times \begin{bmatrix} x-mL \\ y-pL \\ z \end{bmatrix}. \quad (48)$$

Applying (45)–(48) to (26), the tilted beam propagator $\tilde{\mathcal{B}}_{mp}$ in (40) can be written concisely as

$$\tilde{\mathcal{B}}_{mp}(\mathbf{r},\omega) \approx -\Lambda_{mp} i\omega \exp\left(-\frac{\omega^2 T_{mp}^2}{4} + i\omega\tau_{mp}\right)\left(\mathbf{r}-\mathbf{r}'_{mp}\right) \quad (49)$$

where

$$\Lambda_{mp}(\mathbf{r}) = -\frac{L}{\sqrt{2}\pi c R_{mp}^2} \quad (50)$$
$$\tau_{mp}(\mathbf{r}) = c^{-1}\left[z_{bmp} + \frac{\rho_{bmp}^2}{2z_{bmp}} + L\sin\theta_A \cdot (m\cos\phi_A + p\sin\phi_A)\right] \quad (51)$$
$$T_{mp}(\mathbf{r}) = \frac{\rho_{bmp}L\cos\theta_A}{\sqrt{\pi}cz_{bmp}}. \quad (52)$$

In contrast with the 1-D aperture problem [1], the beam propagator in (49) *does not* contain fractional powers of the frequency; therefore, for the class of pulses in (42)–(44), the PB propagator can be evaluated more easily. In particular, by substituting (43), (44) and (49) into (40), and recallling basic properties (differentiation, time-shift) of analytic signals, one obtains

$$\mathbf{b}_{mp}(\mathbf{r},t) = \mathrm{Re}\left[\overset{+}{\mathbf{b}}_{mp}(\mathbf{r},t)\right] = \frac{P_0\Lambda_{mp}\sigma T}{\mathcal{T}_{mp}} \times p_g^{(j+1)}\left[\left(t-\frac{T}{2}-\tau_{mp}\right)\sigma, \mathcal{T}_{mp}\right](\mathbf{r}-\mathbf{r}'_{mp}) \quad (53)$$
$$\mathcal{T}_{mp} = \sqrt{T_{mp}^2 + \sigma^2 T^2}. \quad (54)$$

Thus, the analytic TD narrow-waisted beam expansion in (39) reduces to an efficiently computable closed form in terms of simple analytic functions, with the real field obtained from

$$\mathbf{e}(\mathbf{r},t) = \mathrm{Re}\left[\overset{+}{\mathbf{e}}(\mathbf{r},t)\right] \sim \sum_{m,p}(\mathbf{c}_{mp}\times\mathbf{u}_z)\times\mathbf{b}_{mp}(\mathbf{r},t) \quad (55)$$

Modulated Gaussian pulses can be treated similarly, but require a slightly more complex algebra involving error functions [15].

B. TD Narrow-Waisted Beam Discretization: Nonlinear-Delay Aperture Fields

We now extend the results in Section IV-A to the more general aperture field distribution [cf. (1.52)]

$$\mathbf{f}(x,y,t) = \mathbf{s}(x,y)p\left[t - c^{-1}\Phi(x,y)\right] \quad (56)$$

obtained by Fourier inversion of

$$\mathbf{F}(x,y,\omega) = P(\omega)\mathbf{s}(x,y)\exp\left[i\frac{\omega}{c}\Phi(x,y)\right] \quad (57)$$

where $\mathbf{s}(x,y)$ and $\Phi(x,y)$ are real functions. For moderately nonlinear phasing $\Phi(x,y)$, as discussed in Section III-C for the FD synthesis, it may be convenient to split the phase (delay) function into a linear part plus a nonlinear remainder

$$\Phi(x,y) = \sin\theta_A(x\cos\phi_A + y\sin\phi_A) + \Phi_{NL}(x,y) \quad (58)$$

where $\Phi_{NL}(x,y)$ does not contain linear terms. Referring to (23), $\mathbf{g}(x,y)$ is now given by

$$\mathbf{g}(x,y) = \mathbf{s}(x,y)\exp[ik\Phi_{NL}(x,y)] \quad (59)$$

with the *complex* Gabor coefficients [see (25)]

$$\mathbf{C}_{mp} = \left(\frac{L}{\sqrt{2}}\right)\mathbf{s}(mL,pL)\exp[ik\Phi_{NL}(mL,pL)]. \quad (60)$$

The corresponding TD beam expansion differs slightly from (39) [see (1.57)]

$$\mathbf{e}(\mathbf{r},t) \sim \sum_{m,p}(\mathbf{s}_{mp}\times\mathbf{u}_z)\times\mathbf{b}_{mp}(\mathbf{r},t-t_{mp}) \quad (61)$$

with the PB propagator $\mathbf{b}_{mp}$ taken from (53), and

$$\mathbf{s}_{mp} = \left(\frac{L}{\sqrt{2}}\right)\mathbf{s}(mL,pL), \quad t_{mp} = c^{-1}\Phi_{NL}(mL,pL). \quad (62)$$

For strongly nonlinear phasing, the splitting in (58) offers no computational advantages over the *nontilted* version (i.e., $\theta_A = \phi_A = 0$ in (53)) applied to the entire phase function $\Phi(x,y)$.

C. Assessment of Accuracy

The explicit closed form expressions developed in Section IV-A for the beam propagator integral in (40) are based on a sequence of approximations which have been expressed in terms of interdependent inequalities that involve all relevant problem parameters and are stated in (45) and (47). To systematize estimates of the range of validity in this multiscale problem, it is useful to define a nondimensional (ND) estimator which embodies all of the problem parameters and is structured around specifically scaled ND parameter combinations containing quantities of special interest.

The most stringent overall constraint in (45) and (47) is the *smallness* of the beam parameter b over the whole bandwidth of interest [the second inequality in (47)], which actually determines the maximum allowable lattice period (i.e., the minimum number of beams) for specified Ω, θ_A, and observation point. For specified observation plane at $z = z_{obs}$, recalling that $z_{bmp} = z_{obs}/\cos\theta_A$, this constraint can be written as

$$\frac{(L\cos\theta_A)^2\Omega}{2\pi c} \ll \frac{z_{obs}}{\cos\theta_A}. \tag{63}$$

Multiplying and dividing by $d_A^2 T$ on the right hand side, and introducing the auxiliary ND parameters

$$N_b = \left(\frac{d_A}{L}\right)^2 \text{ (number of beams in (39))} \tag{64}$$

$$\kappa = \frac{\Omega T}{2\pi} \text{ (normalized bandwidth of the pulse)} \tag{65}$$

$$F_d = \frac{d_A^2}{cT} \text{ (Fresnel distance of the aperture)} \tag{66}$$

$$\chi = \frac{z_{obs}}{F_d}, \text{(normalized distance from the aperture)} \tag{67}$$

the constraint in (63) can be written compactly in terms of the ND estimator Q

$$Q \equiv \frac{\kappa(\cos\theta_A)^3}{\chi N_b} \ll 1 \tag{68}$$

which highlights the important role of N_b in the algorithm architecture. Actually, except for square apertures, N_b does not represent the precise number of effective beams (i.e., those with nonzero Gabor coefficients) in the expansion (39), and it should be regarded as a conservative estimate. For robustness, it is required that the number of beams, N_b, is large enough to render the narrow-waisted beam synthesis insensitive to "scramblings" of the beam-lattice parameters, i.e., to different combinations of these parameters within the narrow-waisted constraint. With this in mind, one observes from (68), for example, that decreasing the number of beams N_b can be compensated for by a corresponding increase in χ, i.e., in the observation distance z_{obs} when F_d is specified. In principle, the ND estimator Q in (68) can be used for linear as well as nonlinear delay aperture field distributions (see Section IV-D). However, the actual value of Q ensuring a prescribed accuracy may vary for different distributions. In particular, a finer discretization (i.e., larger N_b) is usually required in the presence of nonlinear phasing/delay, for the same degree of accuracy.

D. Numerical Results

Extensive numerical simulations have been performed in order to validate and calibrate the PB syntheses introduced in Sections IV-A and IV-B. Here we have selected some representative results, comparing the beam syntheses with a reference solution obtained via Gaussian quadrature numerical integration [12] of (3). In all simulations, the aperture field distributions are assumed to be x polarized and therefore [see (3)] the radiated fields contain only x, z components. The assumed temporal excitation is the wideband Rayleigh pulse (four-times differentiated Gaussian) shown in Fig. 7, obtained from (42)–(44) with

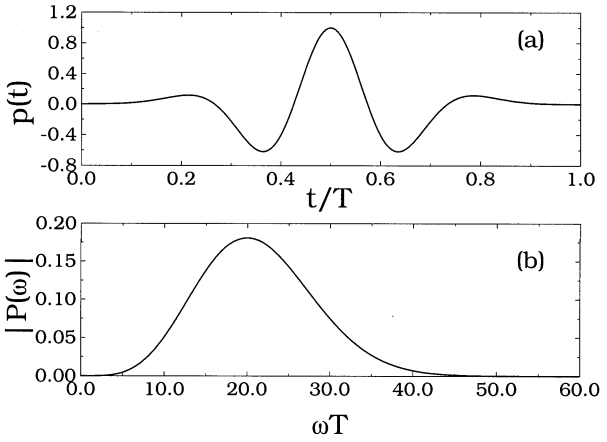

Fig. 7. Rayleigh pulse. (a) Temporal profile in (42). (b) Spectrum (magnitude) in (43) ($j = 4$, $P_0 = T^4/30\,000$, $\sigma = 1/\sqrt{50}$).

$$j = 4, \quad P_0 = \frac{T^4}{30\,000}, \quad \sigma = \frac{1}{\sqrt{50}}. \tag{69}$$

The examples presented below represent the TD counterparts of the FD cases discussed in Section III-D. In all simulations, we used a pulse-bandwidth value $\Omega T = 40$ (see Fig. 7), which sets the reference level for the ND estimator Q.

We first consider the linear-delay aperture field distribution in (34), with $\mathbf{g}(x, y)$ taken as the x polarized, cosine-tapered distribution in (31). Fig. 8 shows typical results for the x component of the radiated field for $\theta_A = 30°$, $\phi_A = 45°$. The problem parameters are listed in the caption. In Fig. 8(a), a grayscale snapshot of the reference field solution is observed in the near-zone of the aperture at a fixed value of z and ct. To highlight details of the PB synthesis in (55), various 1-D cuts of the space-time wavefield are displayed in Fig. 8(b)–(d) for a specified beam lattice period, and are compared with the reference solution. Excellent agreement has been obtained with a relatively small number (20×20) of beams (the two solutions are almost indistinguishible on the scale of the plots); the corresponding value of the nondimensional estimator in (68) is $Q \approx 0.1$. Similar results are observed for the z component in Fig. 9.

The convergence of the PB synthesis and the role of the nondimensional estimator Q are illustrated in Fig. 10, which displays as a function of Q the rms (energy) error $\Delta e_{x,z}$ at fixed observation points $\mathbf{r}$ in the near, intermediate, and far zone of the aperture

$$\Delta e_{x,z} \equiv \frac{\int_{-\infty}^{\infty} \left| e_{x,z}^{(ref)}(\mathbf{r},t) - e_{x,z}^{(beam)}(\mathbf{r},t) \right|^2 dt}{\left[\int_{-\infty}^{\infty} \left| e_{x,z}^{(ref)}(\mathbf{r},t) \right|^2 dt \int_{-\infty}^{\infty} \left| e_{x,z}^{(beam)}(\mathbf{r},t) \right|^2 dt \right]^{1/2}}. \tag{70}$$

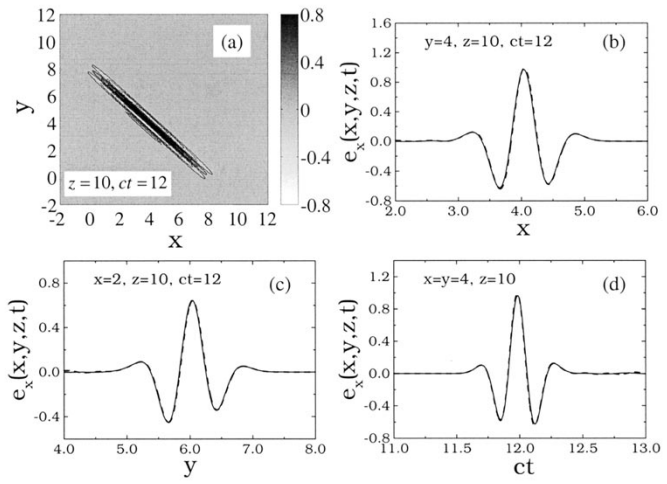

Fig. 8. x polarized, pulsed, linear-delay, square cosine aperture distribution in (34) with (31), $cT = 1$, $d_A = 10 = 10cT$ (arbitrary units), $\theta_A = 30°$, $\phi_A = 45°$: **x component** of radiated field at $z = 10 = 0.1F_d$. (a) Grayscale snapshot of the reference solution (numerical integration of (3)) at $ct = 12$. (b),(c),(d) Cuts at ($y = 4$, $ct = 12$), ($x = 2$, $ct = 12$), and ($x = y = 4$), respectively, comparing the reference solution with the PB beam synthesis (55) ($L = d_A/20$, i.e., 400 beams). For the above parameters, $Q \approx 0.1$. —— Reference solution; – – – Beam synthesis.

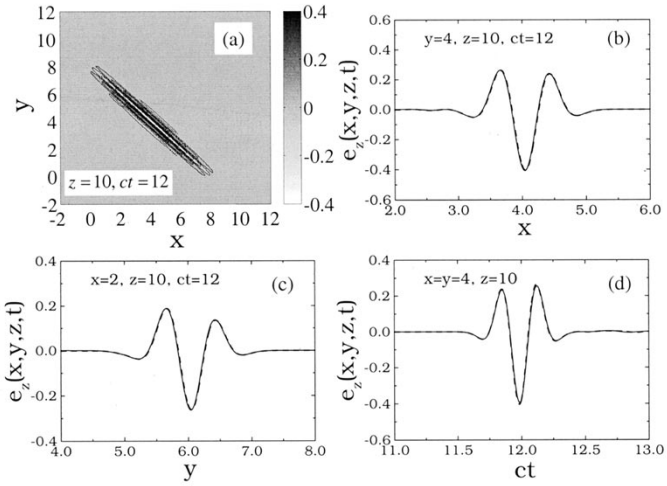

Fig. 9. As in Fig. 8, but **z component**.

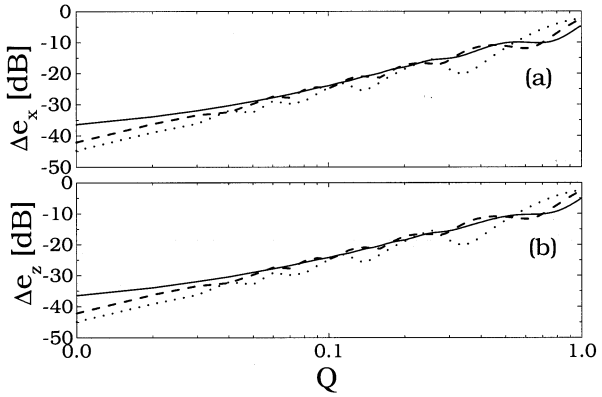

Fig. 10. rms error in (70) for x and z components, respectively, as a function of the nondimensional estimator Q in (68), adjusted by varying N_b. Parameters as in Figs. 8 and 9. Observation points (on the beam axis (θ_A, ϕ_A)): —— $x = y = 4, z = 10 = 0.1F_d$; – – – $x = y = 16, z = 40 = 0.4F_d$; · · · · · · $x = y = 40$, $z = 100 = F_d$.

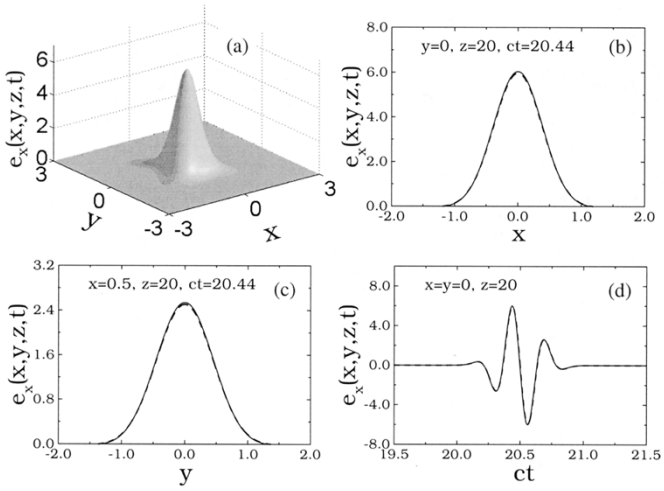

Fig. 11. x polarized, pulsed, focused, square cosine aperture distribution in (71), with $cT = 1$, $d_A = 10 = 10cT$, $L_f = 20 = 0.2F_d$ (arbitrary units). **x component** of radiated field at the focal plane $z = L_f$. (a) Snapshot of the reference solution (numerical integration of (3)) at $ct = 20.44$. (b), (c), (d) Cuts at ($y = 0$, $ct = 20.44$), ($x = 0.5$, $ct = 20.44$), and ($x = y = 0$), respectively, comparing the reference solution with the PB beam synthesis (61) ($L = d_A/80$, i.e., 6400 beams). For the above parameters, $Q \approx 0.05$. —— Reference solution; – – – Beam synthesis.

Each curve in Fig. 10 refers to a fixed observation point, and is parameterized in terms of Q by varying the remaining free parameter in (68), i.e., the number of beams N_b. One observes that the error decreases almost monotonically with decreasing Q (i.e., increasing N_b). Moreover, the error versus Q is *weakly* dependent on the observation distance, confirming our previous experience that, for the same degree of accuracy, a coarser discretization can be used as the observation distance increases, subject to (68). Quantitatively, values of $Q \approx 0.1$ (as in Figs. 8 and 9) yield an error < -20 dB, which is usually acceptable.

As a final example, we consider an x polarized, cosine tapered, aperture distribution with quadratic delay

$$\mathbf{f}(x,y,t) = \mathbf{g}(x,y)p\left[t + \frac{(x^2+y^2)}{(2cL_f)}\right] \tag{71}$$

where $\mathbf{g}(x,y)$ is defined in (31). The above distribution represents the TD counterpart of the FD focusing/defocusing distribution in (33), and constitutes a particularly stringent test for the nonlinear-delay aperture PB synthesis in (61). Fig. 11 contains representative results for the x component of the radiated field, observed in the critical focal plane $z = L_f$ which has been chosen at moderate distance from the aperture, $L_f = 0.2F_d$. In particular, Fig. 11(a) shows a snapshot of the reference solution at the time instant $ct = 20.44$, where the focusing effects are clearly evident. The PB synthesis in (61), for a fixed value of the beam lattice period, is compared with the reference solution in a number of representative 1-D cuts shown in Fig. 11(b)–(d), with excellent agreement. Similar observations apply to the z component of the radiated field in Fig. 12. Note that standard (nonuniform) ray asymptotics would fail due to

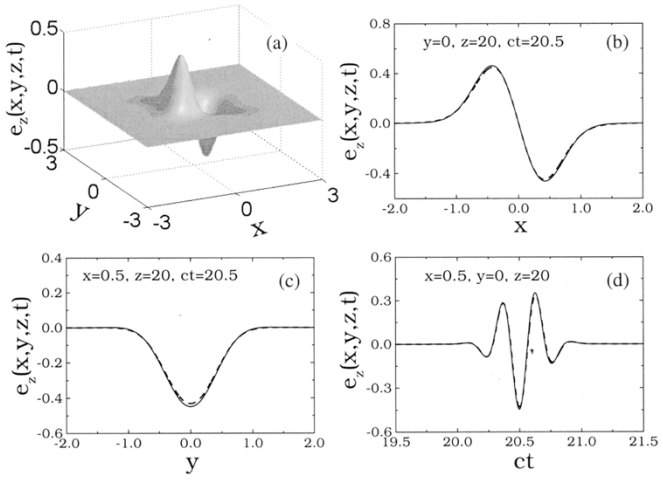

Fig. 12. Parameters as in Fig. 11: **z component**. (a) Snapshot of the reference solution at $ct = 20.5$. (b), (c), (d) Cuts at ($y = 0, ct = 20.5$), ($x = 0.5, ct = 20.5$), and ($x = 0.5,\ y = 0$), respectively, comparing the reference solution with the PB beam synthesis (61) ($L = d_A/80$, i.e., 6400 beams, $Q \approx 0.05$). —— Reference solution; – – – Beam synthesis.

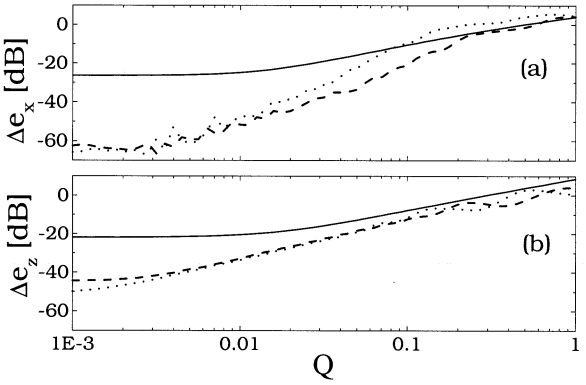

Fig. 13. rms error in (70) for x and z components, respectively, as a function of the nondimensional estimator Q in (68), adjusted by varying N_b. Parameters as in Figs. 11 and12: (a): x component. Observation points: —— $x = y = 0$, $z = 20 = L_f = 0.2F_d$; – – – $x = y = 0$, $z = 70 = 0.7F_d$; · · · · · · $x = y = 0$, $z = 100 = F_d$. (b): z component. Observation points: —— $x = 0.5$, $y = 0$, $z = 20 = L_f$; – – – $x = 3.7$, $y = 0$, $z = 70$; · · · · · · $x = 4.7$, $y = 0$, $z = 100$.

the presence of caustic transition regions. As in the FD case (cf. Section III-D), the narrow-waisted pulsed beams still yield an accurate wavefield synthesis, with an increase (in this example of a factor 16) in the computational effort, as compared with the linear-delay distributions. In this example, we used 80×80 beams, yielding $Q \approx 0.005$. The rms errors in (70) versus Q are shown in Fig. 13 for various observation points. It is observed, for both components, that away from the focal plane $z = L_f$, the error and its numerical values behave similarly to those for the linear-delay case in Fig. 10. In particular, the error behavior is weakly dependent on the observation point. In the more critical focal plane, the error behavior is quite different: it is uniformly larger and reaches a plateau (< -20 dB) for $Q \lesssim 0.005$, indicating an intrinsic lower bound independent of the discretization. Such behavior was not observed in the FD, where the *full* CSP GB propagators are used, and therefore is probably related to the *paraxial* approximation in (46), whose implications are not accounted for in the ND estimator Q [derived from (47)]. For the moderate focusing in this example, this lower bound still yields reasonably accurate syntheses in the focal plane (see Figs. 11 and 12), but for considerably stronger focusing, decreased accuracy can be expected and has actually been encountered in numerical experiments. For these near-zone focal-plane field observations, our numerical simulations usually produced satisfactory accuracy ($\Delta e_{x,z} < -15$ dB) for focused distributions with $L_f > 0.1F_d$. As seen from Fig. 13, reasonable accuracy can be achieved away from the focal plane within the $Q \lesssim 0.1$ constraint observed in the linear-delay case.

The above beam syntheses were obtained with computing times ranging from 2 ms (linearly phased aperture with 400 beams in Figs. 8 and 9) to 32 ms (focused aperture with 6400 beams in Figs. 11 and 12) per space-time sample on a 700 MHz PC. The reference solution was obtained via numerical quadrature of the Kirchhoff integration in (3), using a 7-point Gaussian formula [12] with discretization steps $\Delta_x = \Delta_y = d_A/350 = cT/35$, resulting in computing times of about 600 ms per space-time field sample.

V. Conclusion

Referring for background to the abstract and introduction (Section I), we have developed here a discretized Gabor-based narrow-waisted PB algorithm for synthesis of 3-D vector fields radiated by truncated planar 2-D aperture distributions with amplitude-tapered coordinate-separable linearly and nonlinearly phased profile functions. Building upon the FD 2-D aperture radiation analysis in [2], [3] and the time domain 1-D aperture radiation study in [1], we have obtained the simple, readily computable, robust, explicit asymptotic PB expansions in (55) and (61). Calibration against reference solutions for a variety of numerical test configurations have established the accuracy and range of validity of the PB algorithms. The validity constraints have been formalized through the nondimensional estimator in (68), which combines all relevant problem parameters in terms of physically meaningful spatially and temporally scaled groupings. Computationally, the proposed PB syntheses appear attractive when compared with numerical Kirchhoff integrations, with typical computing times from about 20 to 300 times smaller.

Our next goal is the interaction of the radiated PBs with complex propagation environments. In this connection, forward and inverse scattering applications to 1-D aperture/2-D field configurations have been addressed in [16]–[18]. Extensions to 2-D aperture/3-D field configurations, by combining the PB discretization algorithm in the present paper with Kirchhoff Physical Optics techniques, are currently under consideration.

References

[1] V. Galdi, L. B. Felsen, and D. A. Castañon, "Narrow-waisted Gaussian beam discretization for two-dimensional time-dependent radiation from large apertures," *IEEE Trans. Antennas Propagat.*, vol. 49, pp. 1322–1332, Sept. 2001.

[2] J. J. Maciel and L. B. Felsen, "Discretized Gabor-based beam algorithm for time-harmonic radiation from two-dimensional truncated planar aperture distributions – I: Formulation and solution," *IEEE Trans. Antennas Propagat.*, vol. 50, pp. 1751–1759, Dec. 2002.

[3] ——, "Discretized Gabor-based beam algorithm for time-harmonic radiation from two-dimensional truncated planar aperture distributions – II: Asymptotics and numerical tests," *IEEE Trans. Antennas Propagat.*, vol. 50, pp. 1760–1768, Dec. 2002.

[4] ——, "Systematic study of fields due to extended apertures by Gaussian beam discretization," *IEEE Trans. Antennas Propagat.*, vol. 37, pp. 884–892, July 1989.
[5] ——, "Gaussian beam analysis of propagation from an extended aperture distribution through dielectric layers, Part I – Plane layer," *IEEE Trans. Antennas Propagat.*, vol. 38, pp. 1607–1617, Oct. 1990.
[6] ——, "Gaussian beam analysis of propagation from an extended aperture distribution through dielectric layers, Part II – Circular cylindrical layer," *IEEE Trans. Antennas Propagat.*, vol. 38, pp. 1618–1624, Oct. 1990.
[7] L. B. Felsen and V. Galdi, "Complex-source-point narrow-waisted ray-like Gaussian beams for frequency and time domain radiation and scattering," in *Ultra-Wideband, Short Pulse Electromagnetics 5*, S. R. Cloude and P. D. Smith, Eds. New York: Kluwer/Plenum, Sept. 2002.
[8] V. Galdi, L. B. Felsen, and D. A. Castañon, "Quasiray Gaussian beam algorithm for time-harmonic scattering by moderately rough interfaces," *IEEE Trans. Antennas Propagat.*, vol. 49, pp. 1305–1314, Sept. 2001.
[9] V. Galdi, D. A. Castañon, and L. B. Felsen, "Multifrequency reconstruction of moderately rough interfaces via quasiray Gaussian beams," *IEEE Trans. Geosci. Remote Sensing*, vol. 40, pp. 453–460, Feb. 2002.
[10] V. Galdi, H. Feng, D. A. Castañon, W. C. Karl, and L. B. Felsen, "Multifrequency subsurface sensing in the presence of a moderately rough air-soil interface via quasiray Gaussian beams," *Invited Paper in Radio Science, Special Issue on 2001 URSI EMT Symp.*, vol. 37, no. 6, Nov.-Dec. 2001.
[11] T. B. Hansen and A. D. Yaghjian, *Plane-Wave Theory of Time-Domain Fields: Near-Field Scanning Applications*. Piscataway, NJ: IEEE Press, 1999.
[12] W. H. Press, S. A. Teukolsky, W. T. Vetterling, and B. P. Flannery, *Numerical Recipes in C: The Art of Scientific Computing*, 2nd ed. Cambridge, U.K.: Cambridge Univ. Press, 1992.
[13] L. Wang, C. T. Chen, and W. C. Lin, "An efficient algorithm to compute the complete set of discrete Gabor coefficients," *IEEE Trans. Image Process.*, vol. 3, pp. 87–92, Jan. 1994.
[14] E. Heyman and L. B. Felsen, "Gaussian beam and pulsed beam dynamics: Complex source and spectrum formulation within and beyond paraxial asymptotics," *J. Opt. Soc. Amer. A*, vol. 18, no. 7, pp. 1588–1611, July 2001.
[15] M. Abramowitz and I. A. Stegun, *Handbook of Mathematical Functions*. New York: Dover, 1964.
[16] V. Galdi, L. B. Felsen, and D. A. Castañon, "Quasiray Gaussian beam algorithm for short-pulse two-dimensional scattering by moderately rough dielectric interfaces," *IEEE Trans. Antennas Propagat.*, vol. 51, pp. XXX–XXX, Jan. 2003.
[17] V. Galdi, J. Pavlovich, W. C. Karl, D. A. Castañon, and L. B. Felsen, "Moderately rough dielectric interface reconstruction via short-pulse quasiray Gaussian beams," IEEE Trans. Antennas Propagat., submitted for publication.
[18] V. Galdi, H. Feng, D. A. Castañon, W. C. Karl, and L. B. Felsen, "Moderately rough surface underground imaging via short-pulse quasiray Gaussian beams," IEEE Trans. Antennas Propagat., submitted for publication.

Vincenzo Galdi (M'98) was born in Salerno, Italy, on July 28, 1970. He received the *Laurea* degree (*summa cum laude*) in electrical engineering and the Ph.D. degree in applied electromagnetics from the University of Salerno, in 1995 and 1999, respectively.

From April to December 1997, he held a visiting position in the Radio Frequency Division of the European Space Research Technology Centre (ESTEC-ESA), Noordwijk, The Netherlands, where he was involved in developing CAD tools for microwave filters and phased-array antennas with coaxial excitation. In September 1999, he received a European Union Postdoctoral Fellowship through the University of Sannio, Benevento, Italy. From October 1999 to August 2002, he was a Research Associate with the Department of Electrical and Computer Engineering, Boston University, Boston, MA. In September 2002, he joined the Department of Engineering, University of Sannio, Benevento, Italy, where he is currently an Associate Professor of Electromagnetics. His research interests include analytical and numerical techniques for wave propagation in complex environments, path integrals, and stochastic resonance.

Dr. Galdi is the recipient of a 2001 International Union of Radio Science (URSI) "Young Scientist Award." He is a member of Sigma Xi.

Leopold B. Felsen (S'47–M'54–SM'55–F'62–LF'90) was born in Munich, Germany, on May 7, 1924. He received the B.E.E., M.E.E, and D.E.E. degrees from the Polytechnic Institute of Brooklyn, Brooklyn, NY, in 1948, 1950, and 1952, respectively.

He emigrated to the United States in 1939 and served in the U.S. Army from 1943 to 1946. After 1952, he remained with the Polytechnic (now Polytechnic University), and became University Professor in 1978. From 1974 to 1978 he was Dean of Engineering. In 1994, he resigned from the full-time Polytechnic faculty and was granted the status of University Professor Emeritus. He is now Professor of Aerospace and Mechanical Engineering and Professor of Electrical and Computer Engineering at Boston University, Boston, MA (part-time). He is the author or coauthor of more than 350 papers and of several books, including the classic *Radiation and Scattering of Waves* (Piscataway, NJ: IEEE Press, 1994). He is an Associate Editor of several professional journals and an editor of the *Wave Phenomena Series* (New York: Springer-Verlag). His research interests encompass wave propagation and diffraction in complex environments and in various disciplines, high-frequency asymptotic and short-pulse techniques, and phase-space methods with an emphasis on wave-oriented data processing and imaging.

Dr. Felsen is a member of Sigma Xi and a Fellow of the Optical Society of America and the Acoustical Society of America. He has held named Visiting Professorships and Fellowships at universities in the United States and abroad, including the Guggenheim in 1973 and the Humboldt Foundation Senior Scientist Award in 1981. In 1974 he was an IEEE/APS (Antennas and Propagation Society) Distinguished Lecturer. He was awarded the Balthasar van der Pol Gold Medal from the International Union of Radio Science (URSI) in 1975, an honorary doctorate from the Technical University of Denmark in 1979, the IEEE Heinrich Hertz Gold Medal for 1991, the APS Distinguished Achievement Award for 1998, the IEEE Third Millenium Medal in 2000 (nomination by APS), three Distinguished Faculty Alumnus Awards from Polytechnic University, and an IEEE Centennial Medal in 1984. Also, awards have been bestowed on several papers authored or coauthored by him. In 1977, he was elected to the National Academy of Engineering. He has served on the APS Administrative Committee from 1963–1966, and as Vice Chairman and Chairman for both the United States (1966–1973) and the International (1978–1984) URSI Commission B.

David A. Castañon (S'68–M'79–SM'98) received the B.S. degree in electrical engineering from Tulane University in 1971, and the Ph.D. degree in applied mathematics from the Massachusetts Institute of Technology (MIT), Cambridge, in 1976.

From 1976 to 1981, he was a research associate with the Laboratory for Information and Decision Systems at MIT. From 1982 to 1990, he was Senior and Chief Research Scientist at Alphatech, Inc., Burlington, MA. Since 1990, he has been a Professor with the Department of Electrical and Computer Engineering, Boston University, Boston, MA. His research interests include stochastic control and estimation, optimization, and image processing.

Dr. Castañon served as a member of the Board of Governors of the IEEE Control Systems Society. He is also a member of the AMS, SIAM, and INFORMS.